

# Phase-field modeling of Li-insertion kinetics in single LiFePO<sub>4</sub>-nano-particles for rechargeable Li-ion battery application

Michael Fleck\*

*Metals and Alloys, University Bayreuth,  
Ludwig-Thoma-Straße 36b, 95447 Bayreuth, Germany*

Holger Federmann

*TenneT TSO GmbH, Bernecker Straße 70, 95448 Bayreuth, Germany*

Evgeny Pogorelov

*Advanced Ceramics Group, University Bremen,  
Bibliothekstraße 1, 28359 Bremen, Germany*

## Abstract

We develop a continuum phase-field model for the simulation of diffusion limited solid-solid phase transformations during lithium insertion in LiFePO<sub>4</sub>-nano-particles. The solid-solid phase boundary between the LiFePO<sub>4</sub> (LFP)-phase and the FePO<sub>4</sub> (FP)-phase is modeled as a diffuse interface of finite width. The model-description explicitly resolves a single LiFePO<sub>4</sub>-particle, which is embedded in an elastically soft electrolyte-phase. Furthermore, we explicitly include anisotropic (orthorhombic) and inhomogeneous elastic effects, resulting from the coherency strain, as well as anisotropic (1D) Li-diffusion inside the nano-particle. In contrast to other related research work, we employ an Allen-Cahn-type phase-field approach for the diffuse interface modeling of the solid-solid phase boundary. The model contains an extra non-conserved order parameter field to distinguish the two different phases. The evolution of this order parameter field is controlled by an extra kinetic parameter independent from the Li-diffusion. Further, the effect of the nano-particle's size on the kinetics of FP to LFP phase transformations is investigated by means of both model. Both models predict a substantial increase in the steady state transformation velocity as the particle-size decreases down to dimensions that are comparable with the width of the interface between the FP and the LFP-phase. However, the extra kinetic parameter of the Allen-Cahn-type description may be used to reduce the strength of the velocity-increase with the decreasing particle size. Further, we consider the influence of anisotropic and inhomogeneous elasticity on the lithiation-kinetics within a rectangularly shaped LiFePO<sub>4</sub>-particle embedded in an elastically soft electrolyte. Finally, the simulation of equilibrium shapes of LiFePO<sub>4</sub>-particles is discussed. Within a respective feasibility study, we demonstrate that also the simulation of strongly anisotropic particles with aspect ratios up to 1/5 is possible.

The original research article is available at: <https://doi.org/10.1016/j.commatsci.2018.06.049>

---

\* michael.fleck@uni-bayreuth.de

## I. INTRODUCTION

LiFePO<sub>4</sub> powder is widely considered to be a promising novel cathode material for the application in rechargeable Li-ion batteries. The reasons are high energy storage, low cost and electrochemical stability [1, 2]. Recent trends in the design of LiFePO<sub>4</sub>-cathodes is to synthesize particles of smaller and smaller sizes. For LiFePO<sub>4</sub>-nano-particles excellent performance parameters such as high charge rates have been reported [3]. However, designing next generation Li-ion battery cathodes materials, based on LiFePO<sub>4</sub>-nano-particles, a thorough understanding of the kinetics of the lithiation process in this novel battery material is highly desired. Here, we aim to contribute to this topic from the perspective of a continuum materials science simulation approach. Within the present article we focus on the issues that are placed around the model development, whereas subsequent detailed simulation studies and related results will be part of future work.

The true physical mechanism of the Li insertion process in cathodes made of LiFePO<sub>4</sub> nano-powders is in due to the underlying complexity still a matter of an ongoing scientific debate, and for recent reviews on this issue, we refer to [4, 5]. In this article, the charge and discharge process in the bulk LiFePO<sub>4</sub>-material is regarded to proceed via a coherent solid-solid phase transformation between LiFePO<sub>4</sub> (LFP-phase) and FePO<sub>4</sub> (FP-phase). During this first order phase transformation lithium is inserted into the olivine bulk material. The diffusion of Li inside the orthorhombic olivine lattice is strongly anisotropic along 1D channels in (010) crystallographic direction [6–8]. Important for the modeling of the Li insertion process in single LiFePO<sub>4</sub>-nano-particles is of course the thermodynamics of the bulk LiFePO<sub>4</sub>-system: At room temperature the two stable phases are separated by a miscibility gap, generally providing a strong tendency for the material to phase separate into FP and LFP phase. It is quite interesting that for small LiFePO<sub>4</sub>-particles, a size dependence of the miscibility gap has been observed experimentally [9–11], whereas a relation to the excellent rate capabilities of nano-sized LiFePO<sub>4</sub>-powders is conceivable. It is interesting to note that, such a size dependence of the miscibility gap can result from a gradient energy contribution within diffuse interphase models, where the interface width is on the same order of magnitude than the size of the nano-particle [12–14].

For the development of a respective diffuse-interface description, we apply the so-called phase-field method. This approach has already been applied to model electrochemical reac-

tion kinetics in electrode materials in a number of other research work [13, 15–20]. Within the phase-field method, moving phase boundaries between different phases are treated as diffuse interfaces of finite width. Then, the evolution of the diffuse phase boundary is driven by the mechanics and the thermodynamics of the adjacent bulk phases. In turn, the motion of the diffuse interface strongly influences the bulk properties such as mechanical or thermodynamical degrees of freedom. Already on microscopic length-scale problems, such as solidification or solid-state reactions in metallic alloys, the diffuse interface approach provides an elegant way to dynamically incorporate complex effects, such as multi-component diffusion of refractory elements, chemical reactions at the phase boundary or stress and strain effects due to the lattice mismatch between the phases [21–26]. On the nano-scale, such as in novel  $\text{LiFePO}_4$  cathode materials, the width of the diffuse interface can be chosen in accordance with corresponding experimental observations. In contrast to phase-field descriptions on the micrometer scale, then, the diffuse interface of finite width can carry physical information, which means that the respective nonlinear model behavior has an actual physical meaning [11–14, 27].

Further, we also include anisotropic and inhomogeneous elastic effects, resulting from the lattice misfit between the LFP and the FP-phase. Primarily, these effects are considered to be very important to reproduce experimental observations with regard to favored LFP/FP-interface orientations [16, 28]. Furthermore, it is also interesting to access the micro-mechanical states during the charging of  $\text{LiFePO}_4$ -particles, since frequent cracking along the FP/LFP-interface upon electro-chemical shock is observed and discussed [29–31]. However, a realistic consideration of the elastic effects requires the modeling of the whole particle, which can have strongly anisotropic shapes [32, 33].

Therefore, here, we develop a phase-field model, which combines the following mechanisms for a description of the lithiation-reaction in single  $\text{LiFePO}_4$ -particles:

- The introduction of anisotropic bulk diffusion along 1D channels in (010) crystallographic direction
- The incorporation of anisotropic coherency strains arising from the lattice-mismatch between the two joining solid phases with different elastic constants.
- The implementation of strongly anisotropic interfacial energies that give rise to the anisotropic particle-shapes

- The introduction of the anisotropic particle-shape, which act as a free-surface guaranteeing realistic strain energy contributions

A major difference of the present model, as compared to other models of similar purpose is that the diffusion limited phase transformations are reformulated in terms of two strongly coupled but still independent kinetic equations: one for the Li diffusion and one for the solid-solid phase transformations. This leads to two coupled 2nd order partial differential equations of parabolic type, instead of one equation of forth order. Within the present article, we focus on the model development and discuss the relations and differences to other phase field models for the simulation of charge and discharge in  $\text{LiFePO}_4$  cathodes. Moreover, first interesting results on the size dependent kinetics of diffusion limited phase transformations are presented. Since, an electrolyte phase is explicitly included, it might be also possible to study the complex dynamics of multi-particle interaction [17, 34–36]. However, this is beyond the scope of the present work.

The article is structured as follows: In section II the development of the phase-field model for the kinetic simulation of Li-insertion in single  $\text{LiFePO}_4$  particles is described. It is subdivided into the description of the energetics and the subsequent derivation of the evolution equations. Then, in section III, the simulation results are presented. First, we present the results on the size-dependent kinetics of diffusion limited phase transformations, second the influence of anisotropic and inhomogeneous elastic effects is discussed and finally a feasibility study on the formation of strongly anisotropic particle shapes is presented. Finally, in section IV, a small summary is given.

## II. PHASE FIELD MODELING OF $\text{LiFePO}_4$ PARTICLES

Here, we describe the development of the continuum phase field model for the simulation of lithium insertion kinetics in single  $\text{LiFePO}_4$  nano-particles. In contrast to conventional Cahn-Hilliard-type descriptions, the lithium transport is considered to be independent from the solid-solid phase transformation from the FP-phase to the LFP-phase. The conservative lithium transport is described by a continuous concentration field  $c$ . In order to locally distinguish between the LFP and the FP-phase, we introduce the non-conserved phase field parameter  $\phi$ , with  $\phi = 1$  denoting the LFP phase and  $\phi = 0$  denoting the FP-phase. At the FP/LFP-interface a smooth transition about the phase field width  $\xi_i$  between the two bulk

values of the phase field  $\phi$  is enforced. Furthermore, in the model, we resolve individual nano-particles with the potential possibility to study multi-particle interaction [17, 34–37]. This is realized by the inclusion of an extra phase field  $\varphi$  for the particle, which takes the value  $\varphi = 1$  at the places where a  $\text{LiFePO}_4$ -particle is located and the value  $\varphi = 0$  in the area that surrounds the particles. Finally, the elastic deformations, which result from the lattice-misfit between two the coherently connected phases are contained in the displacement vector-field  $\mathbf{u}$ . All these field are defined in the entire (rectangular) simulation domain. The full 3D-setup of the model for the simulation of lithium insertion in a single anisotropically shaped  $\text{LiFePO}_4$ -particle is illustrated in Fig. 1.

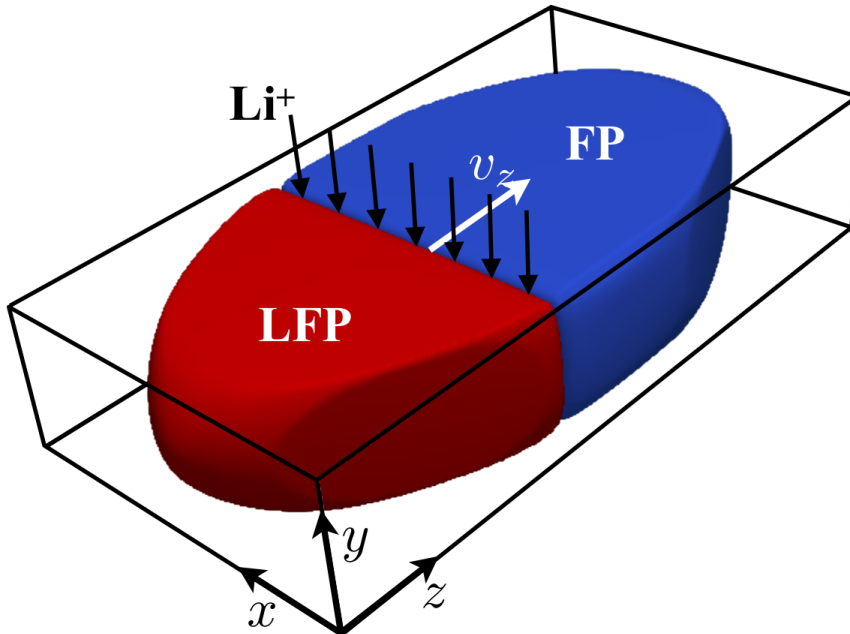


Figure 1. (color online) The setup of a partially lithiated, plate-like particle for the subsequent 3D phase field simulation of the lithiation-reaction inside single  $\text{LiFePO}_4$  nano-particles. The  $\text{LiFePO}_4$ -phase is shown in red and the  $\text{FePO}_4$ -phase in blue. The particle is surrounded by an electrolyte phase, not shown in the picture. Li-diffusion inside the particle is restricted to one-dimensional channels oriented along the (010)-crystallographic orientation as indicated by black arrows.

### A. The energetic formulation

Now we write down the actual phase-field model consisting of the description of the LFP/FP interface, described by  $\phi$ , and the particle-phase boundary, which is denoted as  $\varphi$ .

We start from a phenomenologically motivated Helmholtz free energy functional

$$F = \int dV \left( f_c + f_e + f_i + f_p \right). \quad (1)$$

The first two terms account for thermodynamics and mechanics of the three bulk phases.

$f_c(\phi, \varphi, c)$  denotes the chemical free energy density,

$$f_c = \bar{f}_0 + \frac{\bar{X}}{2} (c - \bar{c}_{eq})^2, \quad (2)$$

which is a quadratic expansion of the free energy density with respect to the local concentration  $c(\mathbf{x}, t)$  of Li<sup>+</sup>-ions, with  $\bar{f}_0(\phi, \varphi)$  being the phase dependent free energy minimum,  $\bar{X}(\phi, \varphi)$  denotes the phase dependent thermodynamic factor, and  $\bar{c}_{eq}(\phi, \varphi)$  denotes the phase dependent concentration of minimal free energy. The second contribution is the elastic free energy density,

$$f_e = \frac{1}{2} (\epsilon_{ik} - \bar{\epsilon}_{ik}^0) \bar{C}_{iklm} (\epsilon_{lm} - \bar{\epsilon}_{lm}^0), \quad (3)$$

where  $\epsilon_{ik} = (\partial u_k / \partial x_i + \partial u_i / \partial x_k) / 2$  denotes the symmetric strain tensor,  $\mathbf{u}(\mathbf{x}, t)$  denotes the displacement vector-field,  $\bar{\epsilon}_{ik}^0(\phi, \varphi)$  is the phase dependent symmetric transformation strain tensor (eigenstrain), and  $\bar{C}_{iklm}(\phi, \varphi)$  denotes the phase dependent stiffness tensor. Note that, according to Einstein's sum convention, the summation over repeated indices is implicitly defined. For any of the mentioned phase dependent physical parameters  $\bar{P} = \bar{X}, \bar{c}_{eq}, \bar{f}_0, \bar{\epsilon}_{ik}^0, \bar{C}_{iklm}$  the phase field dependence is always of the following type,  $\bar{P} = h(\phi)h(\varphi)P^{LFP} + h(1-\phi)h(\varphi)P^{FP} + h(1-\varphi)P^E$ , where  $P^{LFP/FP/E}$  denote respectively the particular bulk value of the specific parameter in the LFP phase, the FP phase and the surrounding electrolyte phase, and  $h(\phi) = \phi^2(3 - 2\phi)$  is the interpolation function. This interpolation function corresponds to the minimal polynomial function satisfying the necessary interpolation condition,  $h(0) = 0$ ,  $h(1) = 1$ , and having also vanishing slope at zero and one, i.e.  $\partial h(\varphi = 0, 1) / \partial \varphi = 0$ , for not to shift the two minima in case of finite driving forces [38].

The last two contributions to the free energy functional are respectively related to the

LFP/FP interface energy and to the surface energy of the particle.

$$f_i = \frac{3\gamma_i\xi_i}{2} (\nabla\phi)^2 + \frac{2\gamma_i}{\xi_i} g(\phi), \quad (4)$$

where  $g(\phi) = \phi^2(1-\phi)^2$  is the double-well-potential, and  $\gamma_i$  as well as  $\xi_i$  denote the interfacial energy as well as the phase field width for the FP to LFP solid solid transformation.

$$f_p = \gamma_p(\nabla\varphi) \left( \frac{3\xi_p}{2} (\nabla\varphi)^2 + \frac{2}{\xi_p} g(\varphi) \right), \quad (5)$$

where  $\gamma_p(\nabla\varphi)$  is the orientation dependent surface energy of the anisotropic particle and similarly  $\xi_p$  denotes the phase field width of the particles surface. Note that the present anisotropic formulation, where the phase-field-gradient dependence is attributed to  $\gamma_p(\nabla\varphi)$ , produces an orientational anisotropy of the interface energy, whereas the phase field width remains isotropic [39].

The functional dependence between the interfacial energy and the orientation is decomposed into a sum of dimensionless facet-functions, which provide a sharp minimum for the respective facet orientation. Therefore the full anisotropy profile is given by the sum over all facet functions:

$$\frac{\gamma_p(\nabla\varphi)}{\gamma_0} = B + \sum_{\mu} \delta_{\mu} \alpha_{\mu}(\nabla\varphi) + \sum_{\nu} \delta_{\nu} \beta_{\nu}(\nabla\varphi), \quad (6)$$

where  $B$  denotes the isotropic background and  $\delta_{\mu/\nu}$  denote respective facet-strengths. Here, two different kinds of functions,  $\alpha_{\mu}(\nabla\varphi)$  and  $\beta_{\nu}(\nabla\varphi)$  are introduced to interpolate the interfacial energy profile in the vicinity of a certain facet orientation. The first anisotropy function is given by

$$\alpha_{\mu}(\nabla\varphi) = - \left( \frac{(n_i^{\mu} \partial_i \varphi)^2}{(\nabla\varphi)^2} \right)^d, \quad (7)$$

with  $\vec{n}^{\nu}$  being the unit vector normal to the plane of the  $\nu$ -th facet and  $d = 128$  is the exponent which allows the orientational minimum to be strongly localized. This function is a generalization of the facet function proposed in [40]. The second anisotropy function is a 3D-generalization of the physically motivated anisotropy profile of Debierr et al. [41]. It is

a stepwise defined function,

$$\beta_\nu(\nabla\varphi) = \begin{cases} (1 - \cos\theta_0 \cos\vartheta^\nu) / \sin\theta_0 & \text{if } \vartheta^\nu > \theta_0, \\ (1 + \cos\theta_0 \cos\vartheta^\nu) / \sin\theta_0 & \text{if } \vartheta^\nu < -\theta_0, \\ \left| \vec{n}^\nu \times \vec{\nabla}\phi \right| / |\nabla\phi| & \text{else,} \end{cases} \quad (8)$$

where  $\cos\vartheta^\nu = \vec{n}^\nu \cdot \vec{\nabla}\varphi / |\nabla\varphi|$  with  $\vec{n}^\nu$  being the unit vector normal to the plane of the  $\nu$ -th facet. Here,  $\theta_0$  denotes the smoothing angle in order to overcome the cusp in the anisotropy profile at the facet orientation  $\vartheta^\nu$ .

## B. The evolution equations

With respect to the modeling of the Li-insertion into single LiFePO<sub>4</sub>-nano-particle the conjointly and coupled motion of the phase fields is not required, as long as the particle morphology does not change during the lithiation, which we will assume in the following. Therefore, we divide the simulation into a sequence of two independent stages: First the formation of the anisotropic particle, and second the lithiation of the finished particle, by means of a transformation from FP to LFP-phase.

The kinetics of the particle formation result from the corresponding Allen-Cahn-equation of motion

$$\begin{aligned} \frac{3\gamma_p \xi_p}{K_p} \frac{\partial\varphi}{\partial t} &= - \left( \frac{\delta F}{\delta\varphi} \right) \\ &= \nabla \left( \frac{\partial f_p}{\partial(\nabla\varphi)} \right) - \frac{\partial f_p}{\partial\varphi} - \frac{\partial f_c}{\partial\varphi}, \end{aligned} \quad (9)$$

where  $K_p$  being the kinetic coefficient for morphological changes of the particles shape. Note that the elastic contribution is omitted here, because we do not consider elastic effects during the formation of the particle. To be able to relax to the equilibrium shape of the particle, we require the conservation of the particle volume. Therefore, we consider the bulk free energy density of the electrolyte phase  $f_0^E$  to be time-dependent in such a way that a volume change



of the electrolyte phase  $V^E$  is prohibited [39, 42]

$$0 = \frac{d}{dt} V^E(t) = \int_V \frac{\partial}{\partial t} (1 - \varphi(\mathbf{x}, t)) dV. \quad (10)$$

Then, inserting the phase field equation (9), the time-dependency of the constant chemical potential density of the electrolyte phase can be calculated as  $f_0^E(t) = R(t)/H(t)$ , where the following abbreviations  $R(t) = K \int_V (\delta F/\delta \varphi) dV$  and  $H(t) = \int_V h'(\varphi) dV$  have been introduced. As shown in [43], this method is also suited for the multi-phase application.

For the second stage, the phase field of the particle  $\varphi$  is treated as constant in time over the whole subsequent simulation of Li-insertion by means of an FP to LFP phase transformation. However, now addressing the FP to LFP solid-state reaction, elastic effects as well as the anisotropic Li-transport both become very important. The Li<sup>+</sup>-ion transport inside a nano-particle is considered to be the rate limiting process, providing the slowest time-scale. The evolution of the local Li<sup>+</sup>-ion concentration is given by the continuity equation

$$\frac{\partial c}{\partial t} = -\frac{\partial}{\partial x_i} \left( M_{ik} \frac{\partial \mu}{\partial x_k} \right), \quad (11)$$

where the ion transport inside the nano-particle is strongly anisotropic, which is reflected by the tensorial mobility  $\mathbf{M}$ . Here,  $\mu$  denotes the non-equilibrium chemical potential, which can be derived from the free energy functional (1) by means of the functional derivative with respect to the concentration,

$$\mu = -\frac{\delta F}{\delta c} = -\bar{X} (c - \bar{c}_{eq}). \quad (12)$$

For the seek of simplicity, we consider the lithium mobility tensor  $\mathbf{M}$  as well as the thermodynamic factor  $X$  to be a phase independent here. Then from the continuity equation (11) as well as Eq. (12) we can derive an equation of motion for the non-equilibrium chemical potential  $\mu$ . We obtain,

$$\frac{\partial \mu}{\partial t} = \frac{\partial}{\partial x_i} \left( D_{ik} \frac{\partial \mu}{\partial x_k} \right) - X \Delta c_{eq} \frac{\partial h}{\partial \phi} \frac{\partial \phi}{\partial t}, \quad (13)$$

where  $\Delta c_{eq} = c_{eq}^{LFP} - c_{eq}^{FP}$  and  $D_{ik} = X M_{ik}$  denotes the lithium diffusivity tensor. The Li-ion transport outside the particle is assumed to be infinity fast leading to a constant ionic

concentration distribution given by the externally applied chemical potential.

The elastic effects result from the lattice-misfit between the LFP and FP phase, which are in the order of a few percent. Restricting to a purely elastic description, we assume the LFP/FP-interface to be coherent. Then, the phase field concept naturally provides the mechanical equilibrium condition: The functional derivative of the free energy functional (1) with respect to the displacements has to vanish,

$$0 = -\frac{\delta F}{\delta u_i} = \frac{\partial}{\partial x_k} \left( \frac{\partial f_e}{\partial \epsilon_{ik}} \right) = \frac{\partial \sigma_{ik}}{\partial x_k}. \quad (14)$$

The stress tensor is naturally defined as the derivative of the elastic free energy density with respect to the strains,  $\sigma_{ik} = \partial f_e / \partial \epsilon_{ik}$ . The electrolyte phase is considered to be elastically weak i.e.  $C_{iklm}^E = 0$ , leading to a stress free surface of the particle.

Finally using variational principles, we obtain the following non-linear partial differential equations for the evolution of the phase field describing the FP to LFP transformations,

$$\frac{1}{K_i} \frac{\partial \phi}{\partial t} = \nabla^2 \phi - \frac{2}{\xi_i^2} g'(\phi) - \frac{1}{3\gamma_i \xi_i} \left( \frac{\partial f_c}{\partial \phi} + \frac{\partial f_e}{\partial \phi} \right), \quad (15)$$

where  $K_i$  is the kinetic coefficient for the solid solid phase transformations.

In summary, the model consists of a set of coupled partial differential equations of second order, as given by the Eq. (9) for the phase field of the particle, the Eq. (13) for the Li diffusion, the Eq. (14) for the elastic displacements and Eq. (15) for the FP to LFP transformations inside the particle. All these equations are solved by finite difference schemes operating on one fixed square grid with explicit Euler-type time integration. With regard to the mechanical (elastic) equilibrium Eq. (14), we perform a Jacobi relaxation. The underlying finite difference scheme is formulated on a staggered grid, as has been further explained in [39, 44, 45].

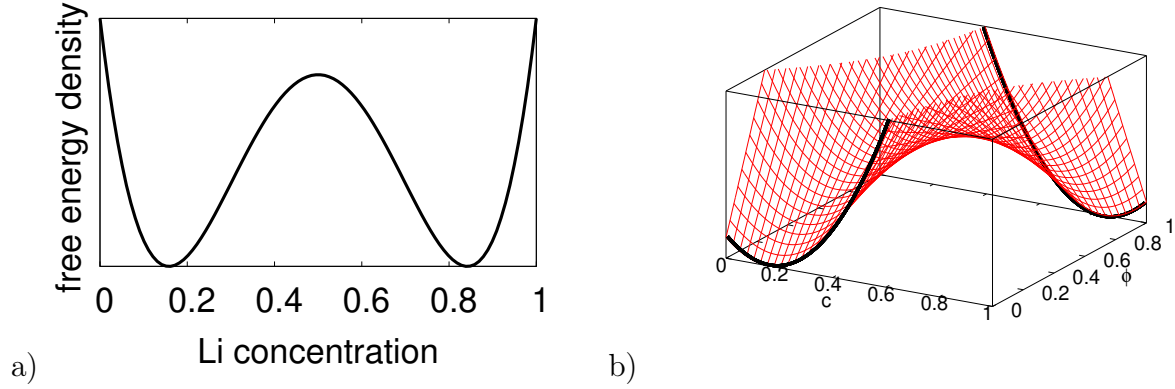


Figure 2. Comparison of the energetic landscape of the two different models: a) the Cahn-Hilliard-type model and b) the Allen-Cahn-type model.

### C. Cahn-Hilliard formulation of FP to LFP transformations

In order to discuss differences and relations between the modeling of the FP to LFP transformations using our new Allen-Cahn-model and conventional Cahn-Hilliard-type formulations, we also consider a respective Cahn-Hilliard-type model. The equivalent Cahn-Hilliard-type formulation of the functional looks as follows

$$F_{CH} = \int dV \left( \frac{U}{2} (\nabla c)^2 + f_c^{CH}(c) \right) \quad (16)$$

where  $f_c^{CH} = X^{CH} (c - c_{eq}^{LFP})^2 (c - c_{eq}^{FP})^2 / 2$  and  $U$  is the gradient energy density. Here,  $X^{CH}$  denotes the thermodynamic factor of the Cahn-Hilliard formulation. The main difference in the energetics is that for the Cahn-Hilliard formulation it is a one dimensional function of the concentration alone, whereas for the Allen-Cahn model it is a two dimensional function of the concentration and the phase-field, as also illustrated in Fig. 2.

Using Eq. (11) as well as the variational definition of the chemical potential Eq. (12), we obtain the Cahn-Hilliard equation

$$\begin{aligned} \frac{\partial c}{\partial t} &= M_{yy} \frac{\partial^2}{\partial x^2} \left( \frac{\delta F}{\delta c} \right), \\ &= M_{yy} \frac{\partial^2}{\partial x^2} \left( \frac{\partial f_c^{CH}}{\partial c} - U \nabla^2 c \right). \end{aligned} \quad (17)$$

The one dimensional equilibrium concentration profile of the Cahn-Hilliard model is given

by

$$c_0(x, t) = \frac{c_{eq}^m}{2} \left( 1 - \frac{\Delta c_{eq}}{c_{eq}^m} \tanh \left( \frac{x - x_0}{\xi_i} \right) \right), \quad (18)$$

with  $c_{eq}^m = c_{eq}^{LFP} + c_{eq}^{FP}$  and  $\Delta c_{eq} = c_{eq}^{LFP} - c_{eq}^{FP}$ . Using this solution, we match the parameters  $U, X^{CH}$  with the respective interface energy  $\gamma_i$  from the Allen-Cahn formulation presented in section II B. Inserting the equilibrium solution (18) into the free energy functional (16), we can evaluate the total free energy density of the LFP/FP interface in the model,

$$\begin{aligned} \gamma_i &= F_{CH}[c_0(x, t)] \\ &= X^{CH} \int_{-\infty}^{+\infty} dx (c_0 - c_{eq}^{FP})^2 (c_0 - c_{eq}^{LFP})^2 \\ &= \frac{\xi_i \Delta c_{eq} X^{CH}}{12} \left( 2 \left( (c_{eq}^{FP})^3 - (c_{eq}^{LFP})^3 \right) + 3 \left( (c_{eq}^{FP})^2 + (c_{eq}^{LFP})^2 \right) \Delta c_{eq} \right), \end{aligned}$$

where we used that  $\partial c_0 / \partial x = 2 (c_0 - c_{eq}^{FP}) (c_0 - c_{eq}^{LFP}) / (\xi_i \Delta c_{eq})$ . From this result, we obtain the condition

$$X^{CH} = \frac{1}{\xi_i \Delta c_{eq}} \frac{12 \gamma_i}{2 \left( (c_{eq}^{FP})^3 - (c_{eq}^{LFP})^3 \right) + 3 \left( (c_{eq}^{FP})^2 + (c_{eq}^{LFP})^2 \right) \Delta c_{eq}}. \quad (19)$$

Further, inserting the equilibrium solution Eq. (18) into the Cahn-Hilliard equation (17), we obtain  $U = \xi_i^2 \Delta c_{eq}^2 X^{CH} / 4$ .

### III. SIMULATION RESULTS

#### A. Diffusion limited FP to LFP phase transformation wave

First, we consider diffusion-limited FP to LFP phase transformations in a rectangular 2D domain, neglecting elastic effects as well as the explicit representation of the electrolyte phase. The relevance of this reduced configuration with regard to the behavior of LiFePO<sub>4</sub>-powders as cathode-material has been discussed previously in the literature [46].

The rectangular 2D domain of size  $L_x \times L_y$  represents a 2D cut of a partially lithiated particle parallel to the [001]-crystallographic plane. The rectangular domain is oriented such that the  $x$ - and  $y$ -coordinate axis meet with the other crystallographic directions

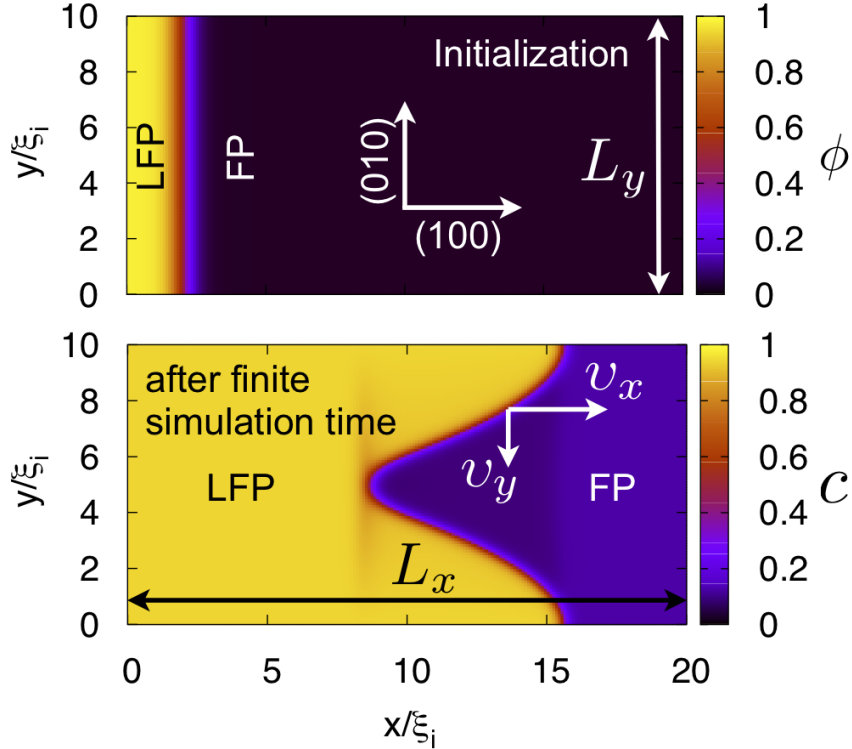


Figure 3. (color online) Setup of the 2D phase field simulations of the lithiation process of a rectangular  $\text{LiFePO}_4$ -particle. On top we show the initial phase field  $\phi$ , and below the Li-ion concentration field after finite simulation time is shown. (LFP denotes the  $\text{LiFePO}_4$ - phase and FP the  $\text{FePO}_4$ -phase)

(100) and (010), respectively, as shown in Fig. 3. Due to the olivine crystal structure, the lithium transport is limited to one dimensional channels along the (010) direction, and it remains only a single non-vanishing element in the mobility tensor, i.e. the  $M_{yy}$ -element. Furthermore, the domain contains finite regions of LFP- and FP-phase, being well separated by a diffuse interface of width  $2\xi_i$ . The lithiation of the 2D-cut of the particle is related to a phase transformation from the lithium poor FP-phase to the lithium rich LFP-phase. The lithiation of the particle is driven by a positive non equilibrium chemical potential  $\mu_0$  applied on the top and bottom boundary of the 2D simulation, which enforces a finite lithium influx into the particle favoring the transformation from FP-phase to LFP.

We start from the FP-phase with a small strip of LFP phase placed on the left side of the system, as shown in Fig. 3. After a certain transient time the system reaches a steady state, where the FP/LFP-interface is moving with a constant velocity and constant shape. For  $L_y \gg \xi_i$ , the interface exhibits a parabolic shaped steady state profile, because the solid phase transformations is limited by the one dimensional lithium diffusion along the

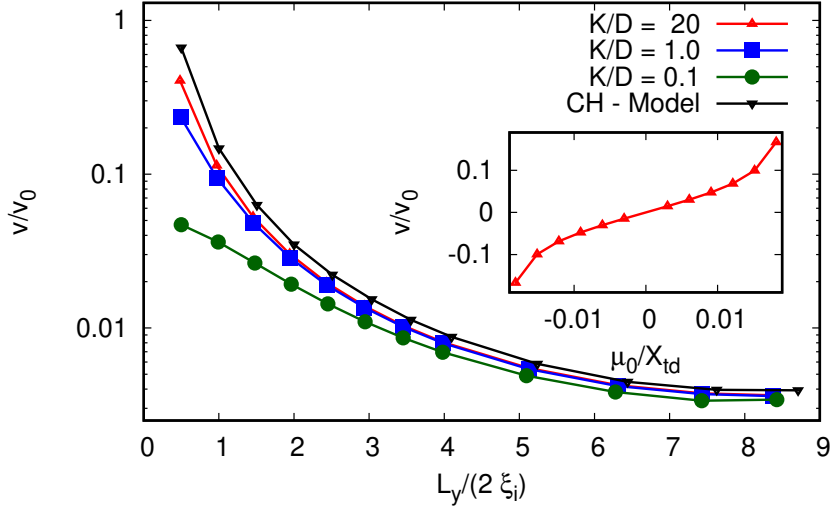


Figure 4. (color online) Change of the steady state interface velocity as function of the particle height  $L_y$ . The velocity is normalized to  $v_0 = D/\xi_i$ . Inset: Dimensionless interface velocity measured under different external potentials  $\mu_0/X_{td}$ .

crystallographic (010)–direction (see Fig. 3). Similar parabolic shaped LFP/FP interfaces have also been reported in other phase-field simulation research-work by Tang et al. [15], who employed a Cahn-Hilliard-type formulation there.

During the simulation, we measure the velocity  $v_x$  of the moving solid solid interface. The resulting steady state velocity is selected by the Li-ion influx through the top and bottom boundary, and is controlled by the imposed external chemical potential  $\mu_0$ . If  $\mu_0$  is chosen to be positive, then Li is transported into the particle, and the LFP-phase starts to grow at the expense of the FP-phase. For  $\mu_0 < 0$  Li-ions are extracted leading to the growth of the FP phase. In the inset of Fig. 4, we plot the measured steady state velocity  $v_0$  as a function of the external potential  $\mu_0$ , for a ratio of the system height to the double of the phase field width of  $L_y/2\xi_i = 1$ . The dimensionless ratio of the thermodynamic factor times the interface width to surface energy has been chosen to be  $X_{td}\xi_i/\gamma_i = 130$ . The velocity is normalized to the characteristic velocity  $v_0 = D/\xi_i$ .

In the main plot of Fig. 4, we show the steady state velocity of the LFP/FP-phase boundary as function of the particle height  $L_y$ , for a ratio of the external chemical potential to the thermodynamic factor of  $\mu_0/X_{td} = 0.01$ . For the dimensionless ratio of the thermodynamic factor times the interface width to surface energy, we again impose  $X_{td}\xi_i/\gamma_i = 130$ .

Generally, we observe an increasing steady state velocity for a decreasing particle-height. And for particles much higher than the width of the diffuse interface region  $\xi_i$ , the velocity becomes independent from the particle height  $L_y$ . Upon a decrease of the dimensionless height from 8 to 1 the Cahn-Hilliard-model predicts a drastic increase of the steady state velocity by nearly two orders of magnitude. Within the Allen-Cahn formulation, a similar velocity-increase is observed, when the phase-field kinetic coefficient  $K$  is chosen to be equally or larger than the Li-diffusion coefficient  $D$ , i.e.  $K/D \geq 1$ . When the imposed value for the kinetic coefficient  $K$  is a factor of ten lower than that of  $D$ , the respective increase of the steady state transformation velocity with decreasing particle height turns out to be respectively smaller. At the same time, the limiting value for the steady state velocity in particles much higher than the phase-field width is found to be nearly independent from the imposed ratio  $K/D$ .

We point out that such an increase of the transformation velocity with a decreasing particle height, is intrinsically related to the underlying diffuse interface description. It has already been reported earlier by Singh et. al, who also did computational studies using a Cahn-Hilliard type phase-field model [46]. However, as compared to the conventional Cahn-Hilliard type description, our Allen-Cahn-type model further allows to control the strength of this velocity-increase, by the respective adjustment of the additional kinetic parameter  $K$ , as shown in the main plot of Fig. 4.

## B. LFP to FP transformations including elastic effects

Next, the full model is applied to the lithiation-kinetics of a rectangularly shaped particle surrounded with a thin layer of the soft electrolyte phase in three dimensions. Here, we also include the effects from the anisotropic and inhomogeneous elastic deformations, which result from the lattice misfit in case of coherent connection between the LFP and the FP phase. The elastic parameters used in the respective simulations are listed in Tab. I. Here, the anisotropic misfit strain reflects the crystallographic shape-change of a unit-volume during the transformation from the orthorhombic  $\text{FePO}_4$ -phase to the also orthorhombic  $\text{LiFePO}_4$ -phase. Here, we distribute the misfit strain symmetrically onto the two different solid phases.

Table I. The elastic parameters used in the simulations of the lithiation of a rectangular particle in three dimensions.

Parameter	LiFePO <sub>4</sub>	FePO <sub>4</sub>	Electrolyte	Dimension	Literature
Stiffness tensor	$C_{11}$	136	171.2	0	GPa
	$C_{22}$	200	141	0	GPa
	$C_{33}$	173	128	0	GPa
	$C_{44}$	35.9	35.7	0	GPa
	$C_{55}$	49.2	45.3	0	GPa
	$C_{66}$	45.0	50.6	0	GPa
	$C_{12}$	73.6	31.3	0	GPa
	$C_{13}$	53.4	55.6	0	GPa
	$C_{23}$	50.5	14.4	0	GPa
Misfit strain	$\epsilon_1^0$	$+2.5 \cdot 10^{-2}$	$-2.5 \cdot 10^{-2}$	0	-
	$\epsilon_2^0$	$+1.8 \cdot 10^{-2}$	$-1.8 \cdot 10^{-2}$	0	-
	$\epsilon_3^0$	$-0.85 \cdot 10^{-2}$	$+0.85 \cdot 10^{-2}$	0	-
	$\epsilon_{4-6}^0$	0	0	0	-

It is calculated from the three different lattice parameters, as follows

$$\begin{aligned} (\epsilon_{ii}^0)^{LFP} &= \frac{a_i^{LFP} - a_i^{FP}}{a_i^{LFP} + a_i^{FP}}, \\ (\epsilon_{ii}^0)^{FP} &= \frac{a_i^{FP} - a_i^{LFP}}{a_i^{LFP} + a_i^{FP}}, \end{aligned}$$

where the index  $i$  denotes one of the three different basic crystallographic orientations. Note, that this definition of the different eigenstrains attributed to the two different solid phases, implies that the elastic reference state corresponds to the arithmetic average of the FP and the LFP. From a physical, important is mainly the different in the eigenstrains of the two phases. Other dimensionless parameters used in these two simulations are  $K/D = 20$ ,  $\mu_0/X_{td} = 0.1$ ,  $X_{td}\xi_i/\gamma_i = 6$  and  $X_{td}/C_{22}^{LFP} = 5$ . The considered configurations are provided in the Figs. 5a) and b), where snapshots of the respective simulations are shown.

In order to visualize the presence of the elastic effects, respectively deformed 0.5-contours of the LFP-phase (red), the FP-phase (blue) as well as the electrolyte-phase (transparent gray) have been plotted. Note that for better visibility the elastic deformations have been magnified by a factor 10. In Fig. 5c), the momentary growth-velocity of the LFP/FP-interface, growing along the  $x$ -direction case a), is compared to the case b), when it grows



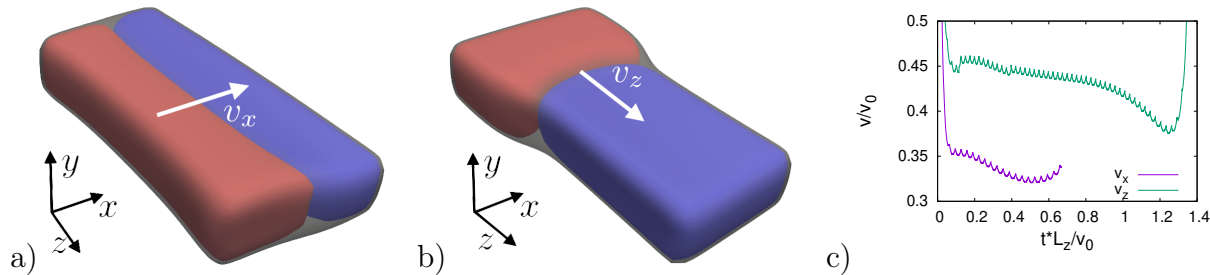


Figure 5. (color online) Snapshots of the different 3D lithiation configurations. a) LFP/FP phase-front is growing along  $x$ -direction. b) LFP/FP phase-front is growing along  $z$ -direction. The elastic deformations due to the anisotropic lattice misfit have been magnified by a factor 10 for better visualization. c) Plot of the momentary interface velocity as measured during the two different simulation. The velocity is normalized to  $v_0 = D/\xi$ .

along the  $z$ -direction. The observed difference in the lithiation-kinetics is related to the influence from the effects the anisotropic and inhomogeneous elasticity, which result from the lattice misfit.

### C. Formation of the anisotropic particle-shape

Further, the lithiation or delithiation kinetics of a single  $\text{LiFePO}_4$ -particle depends on the particle's size and shape in at least two different respects: Coherency strains and stresses as well as diffusion paths are both shape and size dependent. Therefore, a central goal of the modeling has been to include realistic shapes into the model. Experimentally quite a number of different particle shapes are known for the  $\text{LiFePO}_4$ . For example, crystallites have been observed in the shape of hexagonal- or diamond-type platelets [32, 33], rectangular prisms[48], rods and block shapes [49]. Especially the hexagonal- or diamond-type platelets seem to be quite favorable since the due to their large (010)-oriented surface. This surface is normal to the most facile pathway for lithium ion migration, and is hence probably the electrochemically most active one. Further, the thinner the particle in the (010) direction is the shorter are the lithium diffusion paths inside the particle. This may enhance the rate capability of a cathode prepared from such a material [49].

Here, the aim is to generate a strongly anisotropic shape such as the diamond-type platelets-shape, which has been experimentally observed in hydro-thermally synthesized  $\text{LiFePO}_4$  [32]. Unfortunately, such a strongly anisotropic shape can not be produced using Ab-initio-based surface energies. The respectively surface energies for different interface

Table II. The anisotropy parameters used to generate the anisotropic LiFePO<sub>4</sub>-particle shown in Fig. 1

Orientation	Function	Exponent $d$	Amplitude $\delta$
(010)	$\beta(\nabla\varphi)$ ; Eq. (8)	-	5.0
(100)	$\alpha(\nabla\varphi)$ ; Eq. (7)	0	3.0
(100)	$\alpha(\nabla\varphi)$ ; Eq. (7)	5	0.08
(101), ( $\underline{1}$ 01)	$\alpha(\nabla\varphi)$ ; Eq. (7)	5	0.24
(201), ( $\underline{2}$ 01)	$\alpha(\nabla\varphi)$ ; Eq. (7)	5	0.15

orientations are to similar in value to produce the experimentally measured aspect-ratios of 3 to 10 [49, 50]. Therefore, using the anisotropy functions given in Eqs. (7) and (8), an anisotropy profile including some experimentally observed facet-orientations has been designed such that is visually fits to the experimentally observes particle shapes [32]. The anisotropy parameters used in the subsequent phase-field simulation for the particle generation are given in Tab. II. The aim is to get an anisotropic equilibrium shape having an aspect ratio of 1/5 in the yz-cut and having a respectively dominant facet in the (010)-direction. Therefore, first a respectively strong facet has been set in that direction using the anisotropy function from Eq. (8), see the first line of Tab. II. Then, within the xz-cut of the resulting particles, we want an aspect ratio of 1/2, which requires the additional overlay of a smooth anisotropy profile with the orientation (100), such as given by line two of the table. The following lines in Tab. II each provide respective facets at the given orientations respectively on the front and backside of the particle.

In Fig. 6, we compare the resulting 2D cuts of the simulated 3D phase-field with the respective 2D Wulff-construction. For a given anisotropy profile the equilibrium shape is given by Wulff's theorem. The later demands that the particle shape is given by the multitude of all tangents of the  $\gamma_p(\nabla\varphi)$ -plot [51]. Thus, in 2D the equilibrium shape of a particle in parametric form is given by

$$x = \gamma(\vartheta) \cos(\vartheta) - \gamma'(\vartheta) \sin(\vartheta), \quad (20)$$

$$y = \gamma(\vartheta) \sin(\vartheta) + \gamma'(\vartheta) \cos(\vartheta), \quad (21)$$

where  $\vartheta$  is the polar angle. For sufficiently strong anisotropies, the particle equilibrium shape develops sharp corners, where certain high energy orientations are excluded. This is

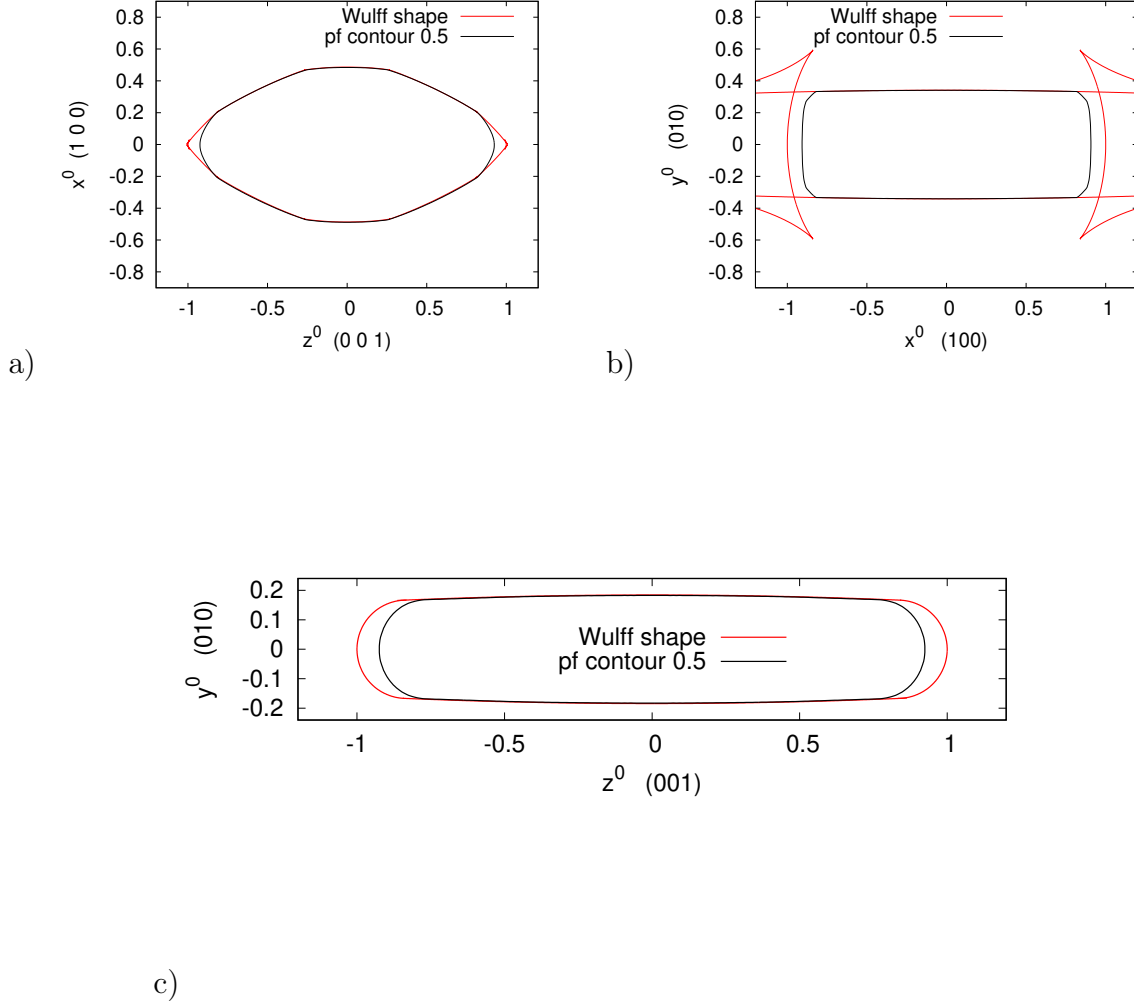


Figure 6. (color online) Comparison of the analytic Wulff-shape with the  $\varphi = 1/2$ -contour of the  $xz$ -cut of the relaxed anisotropic 3D phase field, discriminating between the inner and outer of the  $\text{LiFePO}_4$ -particle. In a) the  $xz$ -cut through the particles mass center is shown, in b) the respective  $xy$ -cut and in c) the  $yz$ -cut.

accompanied by the appearance of the “ears”, i.e. metastable and unstable branches, in the Wulff-construction, as can be also seen in the figure. With regard to the anisotropy profile chosen here, these “ears” are very dominate in the  $xy$ -cut, as shown in Fig. 6b). Generally, with regard to the specific choice of the anisotropy profile, the appearance of ears should be avoided as much as possible, as the phase-field evolution is ill-posed at the respective locations [39, 52, 53].

## IV. CONCLUSION

In summary, we have developed a continuum phase-field model, which takes into account a whole range of mechanisms relevant in the lithiation-reaction in  $\text{LiFePO}_4$  cathode materials, explicitly resolving the particle with its anisotropic shape:

- The introduction of anisotropic bulk diffusion along 1D channels in (010) crystallographic direction
- The incorporation of anisotropic coherency strains arising from the lattice-mismatch between the two joining solid phases with different elastic constants.
- The implementation of strongly anisotropic interfacial energies that give rise to the anisotropic particle-shapes
- The introduction of the anisotropic particle-shape, which act as a free-surface guaranteeing realistic strain energy contributions

A major difference of the presented model, as compared to other models of similar purpose is that the original Cahn-Hilliard-problem was reformulated in terms of two strongly coupled but still independent kinetic equations (diffusion, solid-solid phase transformations). This lead to two coupled 2nd order partial differential equations of parabolic type, instead of one equation of forth order, which is numerically advantageous and leads to the development of kinetic depletion-zones which we regard as physical, and which are not present in the Cahn-Hilliard-type formulation.

Moreover, first interesting results on the size dependent kinetics of diffusion limited phase transformations are presented. The respective simulation study was restricted to a rectangular 2D domain representing a 2D cut of a partially lithiated particle along the (001)-plane and neglecting elastic effects. Then the transformation kinetics is controlled by the external chemical potential  $\mu_0$ , which acts as a driving force for the diffusion limited transformation wave. In the range of small particle thickness in the  $L_y$  direction the simulation studies indicate that  $L_y$  has a strong impact onto the Li-transport into the bulk. In the case of diffusion limited transformations, we observe a strong increase of the resulting steady state velocity, which is related to the difference in the two kinetic time-scales

Finally, we discuss the generation of physically motivated anisotropic particle shapes. From studying experimental particle shapes, we picked out a number of interesting facet-orientations. Then an anisotropy profile was set out for these facet-orientations, and we tuned the respectively calculated Wulff-construction such that is optically fitted to the experimentally observed particle shapes. The resulting anisotropy parameters have been used in the subsequent 3D phase-field simulation for the particle generation. Contours of 2D sections of the resulting phase-field, have been compared to the original 2D Wulff-constructions. This study demonstrates that also the simulation of strongly anisotropic particles with aspect ratios up to 1/5 is possible. Special care, has to be given to the setup of the anisotropy profile, such that the appearance of ears in the Wulff-shape should be avoided as much as possible.

## ACKNOWLEDGMENTS

We thank the Federal Ministry for Economics and Energy (BMWi) of the Federal Republic of Germany for the financial support under the running project COORETEC: ISar (funding code: 03ET7047D). Further, we thank the German Research Foundation for financial support under the DGF Priority Program SPP 1473/1. We acknowledge the financial support from the Oberfranken-Stiftung and the state of Bavaria of the Federal Republic of Germany. Finally, we thank Prof. F. Mertens for the fruitful discussions on the thermodynamic formulation of the model.

## DATA AVAILABILITY

The raw data as well as the processed data required to reproduce these findings are provided within the above text (see for instance Tab. I and Tab. II).

- 
- [1] A. K. Padhi, K. S. Nanjundaswamy, and J. B. Goodenough. Phospho-olivines as Positive-Electrode Materials for Rechargeable Lithium Batteries. *J. Electrochem. Soc.* **144**, 1188 (1997).
  - [2] B. Xu, D. Qian, Z. Wang, and Y. S. Meng. Recent progress in cathode materials research for advanced lithium ion batteries. *Mater. Sci. Eng. Rep.* **73**, 51 (2012).

- [3] B. Kang and G. Ceder. Battery materials for ultrafast charging and discharging. *Nature* **458**, 190–193 (2009).
- [4] R. Malik, A. Abdellahi, and G. Ceder. A critical review of the li insertion mechanisms in lifepo4 electrodes. *Journal of The Electrochemical Society* **160**, A3179 (2013). <http://jes.ecsdl.org/content/160/5/A3179.full.pdf+html>.
- [5] C. T. Love, A. Korovina, C. J. Patridge, K. E. Swider-Lyons, M. E. Twigg, and D. E. Ramaker. Review of lifepo4 phase transition mechanisms and new observations from x-ray absorption spectroscopy. *Journal of The Electrochemical Society* **160**, A3153 (2013). <http://jes.ecsdl.org/content/160/5/A3153.full.pdf+html>.
- [6] M. Tang, W. C. Carter, and Y.-M. Chiang. Electrochemically driven phase transitions in insertion electrodes for lithium-ion batteries: Examples in lithium metal phosphate olivines. *Annu. Rev. Mater. Res.* **40**, 501 (2010).
- [7] S. Nishimura, G. Kobayashi, K. Ohoyama, R. Kanno, M. Yashima, and A. Yamada. Experimental visualization of lithium diffusion in lixfepo4. *Nat. Mater.* **7**, 707 (2008).
- [8] R. Malik, D. Burch, M. Bazant, and G. Ceder. Particle size dependence of the ionic diffusivity. *Nano Lett.* **10**, 4123 (2010).
- [9] M Meethong, H.-Y. S. Huang, W. C. Carter, and Y.-M. Chiang. Size-Dependent Lithium Miscibility Gap in Nanoscale Li<sub>1-x</sub>FePO<sub>4</sub>. *Electrochem. Solid-State Lett.* **10**, A134 (2007).
- [10] P. Gibot, M. Casas-Cabanas, L. Laffont, S. Levasseur, P. Carlach, S. Hamelet, J.-M. Tarascon, and C. Masquelier. Room-temperature single-phase li insertion/extraction in nanoscale lixfepo4. *Nat Mater* **7**, 741 (2008).
- [11] M. Wagemaker, D. P. Singh, W. J. H. Borghols, U. Lafont, L. Haverkate, V. K. Peterson, and F. M. Mulder. Dynamic solubility limits in nanosized olivine lifepo4. *J. Am. Chem. Soc.* **133**, 10222 (2011).
- [12] D. Burch and M. Z. Bazant. Size-dependent spinodal and miscibility gaps for intercalation in nanoparticles. *Nano Letters* **9**, 3795 (2009).
- [13] D. A. Cogswell and M. Z. Bazant. Theory of coherent nucleation in phase-separating nanoparticles. *Nano Letters* **13**, 3036 (2013).
- [14] E. Pogorelov, J. Kundin, and M. Fleck. Analysis of the dependence of spinodal decomposition in nanoparticles on boundary reaction rate and free energy of mixing. *Computational Materials Science* **140**, 105–112 (2017).

- [15] M. Tang, J. F. Belak, and M. R. Dorr. Anisotropic phase boundary morphology in nanoscale olivine electrode particles. *J. Phys. Chem.* **115**, 4922 (2011).
- [16] D. A. Cogswell and M. Z. Bazant. Coherency strain and the kinetics of phase separation in lifepo4 nanoparticles. *ACS Nano* **6**, 2215 (2012).
- [17] B. Orvananos, H.-C. Yu, A. Abdellahi, R. Malik, C. P. Grey, G. Ceder, and K. Thornton. Kinetics of nanoparticle interactions in battery electrodes. *Journal of The Electrochemical Society* **162**, A965 (2015). <http://jes.ecsdl.org/content/162/6/A965.full.pdf+html>.
- [18] L. Liang, Y. Qi, F. Xue, S. Bhattacharya, S. J. Harris, and L. Q. Chen. Nonlinear phase-field model for electrode-electrolyte interface evolution. *Phys. Rev. E* **86**, 051609 (2012).
- [19] J. E. Guyer, W. J. Boettinger, J. A. Warren, and G. B. McFadden. Phase field modeling of electrochemistry. II. Kinetics. *Phys. Rev. E* **69**, 021604 (2004).
- [20] S. Hu, Y. Li, K. M. Rosso, and M. L. Sushko. Mesoscale phase-field modeling of charge transport in nanocomposite electrodes for lithium-ion batteries. *The Journal of Physical Chemistry C* **117**, 28–40 (2013).
- [21] M. Asta, C. Beckermann, A. Karma, W. Kurz, R. Napolitano, M. Plapp, G. Purdy, M. Rappaz, and R. Trivedi. Solidification microstructures and solid-state parallels: Recent developments, future directions. *Acta Mater.* **57**, 941–971 (2009).
- [22] H. Emmerich. Advances of and by phase-field modelling in condensed-matter physics. *Adv. Phys.* **57**, 1 (2008).
- [23] I. Steinbach. Phase-field models in materials science. *Modelling Simul. Mater. Sci. Eng.* **17**, 073001 (2009).
- [24] Y. Wang and J. Li. Phase field modeling of defects and deformation. *Acta Mater.* **58**, 1212 (2010).
- [25] M. Fleck, F. Querfurth, and U. Glatzel. Phase field modeling of solidification in multi-component alloys with a case study on the Inconel 718 alloy. *J. Mater. Res.* **32**, 4605–4615 (2017).
- [26] L.T. Mushongera, M. Fleck, J. Kundin, Y. Wang, and H. Emmerich. Effect of re on directional  $\gamma'$ -coarsening in commercial single crystal ni-base superalloys: A phase field study. *Acta Mater.* **93**, 60 (2015).
- [27] M. Tang and A. Karma. Surface modes of coherent spinodal decomposition. *Phys. Rev. Lett.* **108**, 265701 (2012).

- [28] A. Van der Ven, K. Garikipati, S. Kim, and M. Wagemaker. The role of coherency strains on phase stability in lixfepo4: Needle crystallites minimize coherency strain and overpotential. *Journal of The Electrochemical Society* **156**, A949–A957 (2009).
- [29] M. Zhu, J. Park, and A. M. Sastry. Fracture analysis of the cathode in li-ion batteries: A simulation study. *Journal of The Electrochemical Society* **159**, A492 (2012).
- [30] W. H. Woodford, W. C. Carter, and Y.-M. Chiang. Design criteria for electrochemical shock resistant battery electrodes. *Energy Environ. Sci.* **5**, 8014 (2012).
- [31] W. H. Woodford, Y.-M. Chiang, and W. C. Carter. Electrochemical Shock of Intercalation Electrodes: A Fracture Mechanics Analysis. *Journal of The Electrochemical Society* **157**, A1052 (2010).
- [32] G. Chen, X. Song, and T.J. Richardson. Electron microscopy study of the lifepo4 to fepo4 phase transition. *Electrochem. Solid-State Lett.* **9**, A295–289 (2006).
- [33] X. Qin, J. Wang, J. Xie, F. Li, L. Wen, and X. Wang. Hydrothermally synthesized lifepo4 crystals with enhanced electrochemical properties: simultaneous suppression of crystal growth along [010] and antisite defect formation. *Phys. Chem. Chem. Phys.* **14**, 2669 (2012).
- [34] W. Dreyer, C. Gohlke, and R. Huth. The behavior of a many-particle electrode in a lithium-ion battery. *Physica D: Nonlinear Phenomena* **240**, 1008 (2011).
- [35] W. Dreyer, J. Jamnik, C. Gohlke, R. Huth, J. Moskon, and M. Gaberscek. The thermodynamic origin of hysteresis in insertion batteries. *Nat. Mat.* **9**, 448 – 453 (2010).
- [36] B. Orvananos, T. R. Ferguson, H.-C. Yu, M. Z. Bazant, and K. Thornton. Particle-level modeling of the charge-discharge behavior of nanoparticulate phase-separating lithium battery electrodes. *Journal of The Electrochemical Society* **161**, A535 (2014). <http://jes.ecsdl.org/content/161/4/A535.full.pdf+html>.
- [37] Y. Li, F. El Gabaly, T. R. Ferguson, R. B. Smith, N. C. Bartelt, J. D. Sugar, K. R. Fenton, D. A. Cogswell, A. L. D. Kilcoyne, T. Tyliczszak, M. Z. Bazant, and W. C. Chueh. Current-induced transition from particle-by-particle to concurrent intercalation in phase-separating battery electrodes. *Nat Mater* **13**, 1149 (2014).
- [38] K. Kassner, C. Misbah, J. Müller, J. Kappey, and P. Kohlert. Phase-field modeling of stress-induced instabilities. *Phys. Rev. E* **63**, 036117 (2001).
- [39] M. Fleck, L. Mushongera, D. Pilipenko, K. Ankit, and H. Emmerich. On phase-field modeling with a highly anisotropic interfacial energy. *Eur. Phys. J. Plus* **126**, 95 (2011).



- [40] T. Uehara and R. F. Sekerka. Phase field simulations of faceted growth for strong anisotropy of kinetic coefficient. *J. of Cryst. Growth* **254**, 251 (2003).
- [41] J.-M. Debierre, A. Karma, F. Celestini, and R. Guérin. Phase-field approach for faceted solidification. *Phys. Rev. E* **68**, 041604 (2003).
- [42] A. Karma and W.-J. Rappel. Quantitative phase-field modeling of dendritic growth in two and three dimensions. *Phys. Rev. E* **57**, 4323 (1998).
- [43] B. Nestler, F. Wendler, M. Selzer, B. Stinner, and H. Garcke. Phase-field model for multiphase systems with preserved volume fractions. *Phys. Rev. E* **78**, 011604 (2008).
- [44] D. Pilipenko, M. Fleck, and H. Emmerich. On numerical aspects of phase-field fracture modelling. *Eur. Phys. J. Plus* **126**, 100 (2011).
- [45] M. Fleck. *Solid-state transformations and crack propagation: a phase field study*. Ph.D. thesis, RWTH Aachen, Institut für Festkörperforschung, Theorie der Strukturbildung, Forschungszentrum Jülich (2011). URL <http://darwin.bth.rwth-aachen.de/opus3/volltexte/2011/3511/>.
- [46] G. K. Singh, G. Ceder, and M. Z. Bazant. Intercalation dynamics in rechargeable battery materials: General theory and phase-transformation waves in lifepo4. *Electrochimica Acta* **53**, 7599 (2008).
- [47] T. Maxisch and G. Ceder. Elastic properties of olivine  $\text{Li}_x\text{FePO}_4$  from first principles. *Phys. Rev. B* **73**, 174112 (2006).
- [48] B. Ellis, Wang Hay Kan, W. R. M. Makahnouk, and L. F. Nazar. Synthesis of nanocrystals and morphology control of hydrothermally prepared  $\text{LiFePO}_4$ . *J. Mater. Chem.* **17**, 3248 (2007).
- [49] C. A. J. Fisher and M. S. Islam. Surface structures and crystal morphologies of lifepo4: relevance to electrochemical behaviour. *J. Mater. Chem.* **18**, 1209 (2008).
- [50] L. Wang, F. Zhou, Y. S. Meng, and G. Ceder. First-principles study of surface properties of *lifepo4* : Surface energy, structure, wulff shape, and surface redox potential. *Phys. Rev. B* **76**, 165435 (2007).
- [51] W. K. Burton, N. Cabrera, and F. C. Frank. The growth of crystals and the equilibrium structure of their surfaces. *Phil. Trans. R. Soc. Lond. A* **243**, 299 (1951).
- [52] J. E. Taylor and J. W. Cahn. Diffuse interfaces with sharp corners and facets: Phase field models with strongly anisotropic surfaces. *Physica D* **112**, 381 (1998).

- [53] J. J. Eggleston, G. B. McFadden, and P. W. Voorhees. A phase-field model for highly anisotropic interfacial energy. *Physica D* **150**, 91 (2001).